(Received 10 November 2025, Accepted 25 December 2025, Scheduled 12 January 2026)

# Solution of One-Hop Sky-Wave Field of Arbitrarily Oriented LF Electric Dipole in the Planar Stratified Earth-Ionosphere Waveguide

Xinyue Hu[1], Lili Zhou[1,*], Zhonglin Mu[2], Ying Zhang[1], and Jinsheng Zhang[3]

[1] *The School of Electronic Information and Artificial Intelligence Shaanxi University of Science and Technology, Xi'an 710021, China*
[2] *Aviation Engineering School of Air Force Engineering University, Xi'an 710038, China*
[3] *The College of Missile Engineering, Rocket Force University of Engineering, Xi'an 710025, China*

**ABSTRACT:** In this paper, a method is proposed for solving the one-ho sky-wave propagation problems of an arbitrarily oriented low-frequency (LF) electric dipole within a planar layered Earth-ionosphere waveguide. The purpose of this study is to clarify the relationship between the radiation field and the direction of the electric dipole source in a planar-layered Earth-ionosphere waveguide. In deriving the specific formulas, we employed an ideal far-field approximation idea for an arbitrarily oriented electric dipole in free space and the method of images in layered media. The reflection characteristics of different polarized plane waves at the interface were also taken into account. Based on the improved wave-hop theory, the expressions for the one-hop sky-wave field excited by dipole sources with different directions suitable for an irregular surface are further derived. Using the proposed method, we calculated the sky-wave fields of electric dipoles operating at 100 kHz with various orientations at different receiver altitudes. The results show that the proposed method can be conveniently used to analyze the one-hop sky-wave field of the electric dipole sources with various orientations in a planar stratified Earth-ionosphere waveguide and provides an efficient modeling tool for the LF communication system design and signal prediction over complex terrain

## 1. INTRODUCTION

Low-frequency (LF, 30–300 kHz) radio waves, owing to their long wavelengths, exhibit distinctive advantages such as low attenuation, strong anti-interference capability, and stable long-distance propagation, making them highly important in scientific research and engineering applications [1]. Currently, they are widely used in key technical domains such as navigation and timing, short-term earthquake prediction, lightning location, and underwater communication [2–4]. The propagation characteristics of LF waves significantly influence the performance of these systems [1]. Research on the propagation characteristics of different radio-wave modes in stratified waveguides (such as the Earth-ionosphere waveguide) has attracted increasing attention [5, 6].

Radio-wave radiation sources can be categorized into two types: artificial sources (e.g., high-power transmitters) and natural sources (e.g., lightning and geophysical activities). Compared to artificial sources, which usually emit radiation in a fixed direction, natural sources generally exhibit radiation characteristics in an arbitrary direction [7]. Given that the physical size of the LF source is usually much smaller than the wavelength, the transmitting antenna can be generally equivalent to a horizontal or a vertical electric dipole. In Earth-ionosphere waveguides, radio waves usually propagate in two ways: ground waves and sky waves [8, 9]. As one of the most basic radiation elements, the solution of the horizontal/vertical dipole field in a planar or spherical stratified region has long been a popular research topic [10–18]. Many formulas have been recorded for the field excited by LF vertical electric dipoles in the Earth-ionosphere waveguide, such as the classical waveguide mode method and the wave-hop method recommended by the International Radio Consultative Committee (CCIR) (rec. ITU-R p.684-7) [8, 9]. However, there are relatively few derivations of the sky-wave field of LF horizontal electric dipoles. In [16], based on the reciprocity principle, the ground-wave and sky-wave fields radiated by an LF horizontal electric dipole in the Earth-ionosphere are given, and the expressions of the one-hop and two-hop sky-wave fields are presented concerning the recommended method of CCIR. However, when calculating the sky-wave field of the horizontal electric dipole, the simplified expression used is almost the same as that of the vertical dipole radiation field, except that an additional cosine factor is associated with dipole orientation.

In 2021, we improved the method for calculating the LF one-hop sky-wave field generated by a vertical electric dipole in a stratified planar Earth-ionosphere waveguide [19]. Although the process accounts for the influence of surface irregularities, it is confined to vertical dipoles and cannot be extended to other orientations. Building upon this work, we further expand the scope to focus on the radiation field of arbitrarily oriented electric dipoles in a planar stratified Earth-ionosphere waveguide.

* Corresponding author: Lili Zhou (zhoulili@sust.edu.cn).

This extension has a clear physical significance and application value. For instance, actual radiation sources, such as lightning, often exhibit complex, arbitrary polarization directions, yet a convenient, unified analytical method for the sky-wave fields they excite is lacking. Specifically, in this study, by combining the decomposition of the radiation field from an arbitrarily oriented dipole in free space, the image method for the stratified waveguide, and a rigorous analysis of the reflection characteristics of different polarized plane waves at the boundaries of the ionosphere and ground, a general calculation formula suitable for an arbitrarily oriented dipole is derived. In this study, two representative types of emission sources were considered: Loran-C signal sources and sinusoidal signal sources. Based on their distinct signal characteristics, the variation of the one-hop sky-wave field strength was systematically analyzed by using different appropriate observation methods.

## 2. THEORETICAL MODEL AND METHOD

In this section, formulas are derived to solve the one-hop sky-wave fields excited by an arbitrarily oriented electric dipole in a planar stratified Earth-ionosphere waveguide. Considering that the ground and ionosphere are homogeneous and isotropic media, we established a three-layer waveguide model consisting of the ionosphere, air, and ground from top to bottom, as shown in Figure 1. The relative permittivities of the ionosphere, air, and ground are denoted as $\varepsilon_{rs}$, $\varepsilon_r$, and $\varepsilon_{rg}$. The conductivities are expressed as $\sigma_s$, $\sigma$, and $\sigma_g$, respectively. The vertical distance between the lower boundary of the ionosphere and the Earth's surface is $H$. Taking the spherical coordinate system, the electric dipole $Il$ is assumed to be on the surface at the origin $O$, and the unit vector in its direction is $\hat{e}_{r_0}$, $Il = \hat{e}_{r_0} Il$. The coordinate points corresponding to the unit vector $\hat{e}_{r_0}$ in the spherical coordinate system is $(1, \varphi_0, \theta_0)$. The unit vectors in the other two directions orthogonal to $\hat{e}_{r_0}$ are $\hat{e}_{\varphi_0}$ and $\hat{e}_{\theta_0}$, respectively. The coordinates of the observation position are $(r, \varphi, \theta)$. The great-circle distance between the observation point $R$ and source $O$ on the $xOy$ plane is $d$.

When the dipole source is on the ground, and the distance between the observation point and ground is $h_0$, there are two types of one-hop sky-wave propagation paths at $R$ as shown in Figure 1. Suppose that the first electric field component $\mathbf{E}_1$ comes from the propagation path $\widehat{OPR}$ (Ray 1) with geometric length $L_1$, and the second component $\mathbf{E}_2$ comes from path $\widehat{OP'QR}$ (Ray 2) with length $L_2$. As shown in Figure 1, $\mathbf{E}_1$ experiences one ionospheric reflection during its propagation, and $\mathbf{E}_2$ experiences one ionospheric reflection and one ground reflection. The angles between the two rays ($\widehat{OP}$ and $\widehat{OP'}$) and $z$-axis are $\theta_1$ and $\theta_2$, respectively. According to Figure 1, for radio waves propagating over a homogeneous flat surface, we readily find that

$$\begin{cases} \theta_{1,2} = \arctan\left[d/\left(2H \mp h_0\right)\right] \\ L_{1,2} = d/\sin\theta_{1,2}. \end{cases} \tag{1}$$

Define $R'$ as the image point of $R$ with respect to the lower boundary of the ionosphere. In the spherical coordinate system, the unit vectors corresponding to the three orthogonal directions at point $R$ are $\hat{e}_r$, $\hat{e}_\varphi$, and $\hat{e}_\theta$. The unit vectors corresponding to the three orthogonal directions at point $R'$ are $\hat{e}_{r_1}$, $\hat{e}_{\varphi_1}$, and $\hat{e}_{\theta_1}$, respectively, as shown in Figure 1. Due to the symmetry between $R$ and $R'$ in the planar waveguide model, the azimuth angle remains unchanged, yielding $\hat{e}_{\varphi 1} = \hat{e}_\varphi$. Assuming that the direct-wave electric field of the dipole $\hat{e}_{r_0} Il$ (located at $O$) at the image point $R'$ in the far-field zone is $\mathbf{E}_{d_1}$ (the radio wave propagates in pure air), it can be proven that the direction vector of $\mathbf{E}_{d_1}$ can be expressed as $\hat{e}_{r_1} \times (\hat{e}_{r_0} \times \hat{e}_{r_1})$. The corresponding electric field expression is given by [17]:

$$\mathbf{E}_{d_1} = \hat{\mathbf{e}}_{r_1} \times (\hat{\mathbf{e}}_{r_0} \times \hat{\mathbf{e}}_{r_1})\, \mathrm{i}\omega\mu Il e^{\mathrm{i}kL_1}/(4\pi L_1) \tag{2}$$

The direction vector $\hat{e}_{r_1} \times (\hat{e}_{r_0} \times \hat{e}_{r_1})$ is first expanded in terms of $\hat{e}_{r_0}$, $\hat{e}_{\varphi_1}$, and $\hat{e}_{\theta_1}$. To facilitate the subsequent analysis of reflection at the air-ionosphere interface, $\hat{\mathbf{e}}_{\theta_1}$ is transformed into Cartesian coordinates $(\hat{\mathbf{e}}_x, \hat{\mathbf{e}}_y, \hat{\mathbf{e}}_z)$ [18]. Consequently, the complete expression for the direct-wave field $\mathbf{E}_{d_1}$ at $R'$ is obtained as follows:

$$\begin{aligned} \mathbf{E}_{d_1} = \{&(\hat{\mathbf{e}}_x \cos\theta_1 \cos\varphi + \hat{\mathbf{e}}_y \cos\theta_1 \sin\varphi - \hat{\mathbf{e}}_z \sin\theta_1) \\ &\cdot [\sin\theta_0 \cos\theta_1 \cos(\varphi - \varphi_0) - \cos\theta_0 \sin\theta_1] \\ &+ \hat{\mathbf{e}}_\varphi [-\sin\theta_0 \sin(\varphi - \varphi_0)]\}\mathrm{i}\omega\mu Il\, \mathrm{e}^{\mathrm{i}kL_1}/(4\pi L_1). \end{aligned} \tag{3}$$

Based on the boundary conditions for oblique incidence at the air-ionosphere interface (depicted in Figure 1), we derive that the reflected field components of the parallel-polarized wave (where the electric field is parallel to the plane of incidence) in the $\hat{e}_x$ and $\hat{e}_y$ directions reverse their signs relative to the incident field [17]. The component of the reflected field along the $z$-axis ($\hat{e}_z$) remains unchanged. Then, according to the time-harmonic convention $e^{-i\omega t}$ (where $\omega$ is the angular frequency), the first sky-wave field component $\mathbf{E}_1$ at $R$ can be expressed as

$$\begin{aligned} \mathbf{E}_1 = \{&(-\hat{\mathbf{e}}_x \cos\theta_1 \cos\varphi - \hat{\mathbf{e}}_y \cos\theta_1 \sin\varphi - \hat{\mathbf{e}}_z \sin\theta_1) \\ &\cdot [\sin\theta_0 \cos\theta_1 \cos(\varphi - \varphi_0) - \cos\theta_0 \sin\theta_1] R_{s\parallel}(\theta_1) + \hat{\mathbf{e}}_\varphi \\ &\cdot [-\sin\theta_0 \sin(\varphi - \varphi_0)] R_{s\perp}(\theta_1)\}\mathrm{i}\omega\mu Il \mathrm{e}^{\mathrm{i}kL_1}/(2\pi L_1). \end{aligned} \tag{4}$$

where $R_{s\parallel}(\theta_1)$ and $R_{s\perp}(\theta_1)$ denote the Fresnel reflection coefficients for parallel-polarized and perpendicular-polarized plane waves on the air-ionosphere interface, and $\theta_1$ is the angle of incidence. Then, leveraging the transformation from Cartesian to spherical coordinates [8, 9], we transform the Cartesian field components $\hat{e}_x$, $\hat{e}_y$, and $\hat{e}_z$ in (4) into

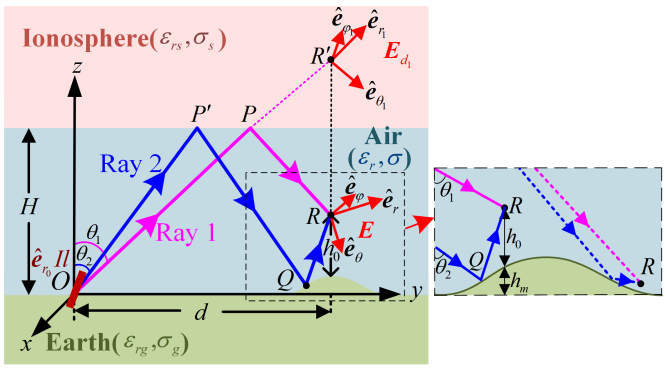


**FIGURE 1**. Planar stratified Earth-ionosphere waveguide model.

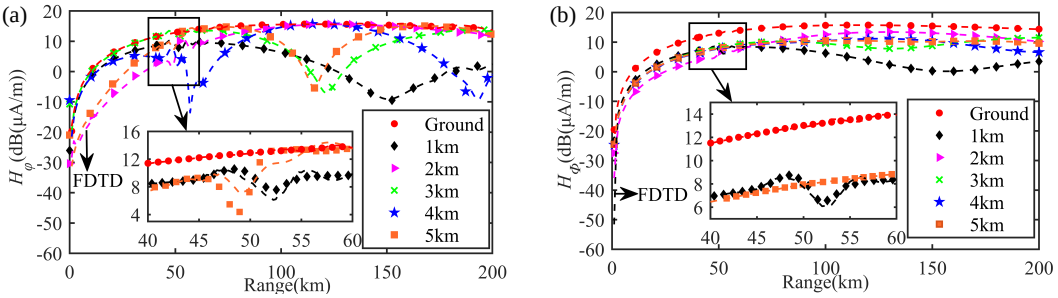


**FIGURE 2**. The one-hop sky-wave magnetic fields $H_\varphi$ excited by the vertical dipole in the irregular Earth-ionosphere waveguide. (a) Sinusoidal signal. (b) Loran-C signal.

the spherical coordinate basis $\hat{e}_\theta$ and $\hat{e}_r$ again. The term $(-\hat{\mathbf{e}}_x \cos\theta_1 \cos\varphi - \hat{\mathbf{e}}_y \cos\theta_1 \sin\varphi - \hat{\mathbf{e}}_z \sin\theta_1)$ can be rewritten as $[-\hat{\mathbf{e}}_r \sin(\theta + \theta_1) - \hat{\mathbf{e}}_\theta \cos(\theta + \theta_1)]$. The $\hat{\mathbf{e}}_\varphi$ component remains unchanged because it is a spherical unit vector. The field component $\mathbf{E}_1$ is thereby rewritten in the spherical coordinate basis as follows:

$$\begin{aligned}\mathbf{E}_1 = \{&[-\hat{\mathbf{e}}_r \sin(\theta+\theta_1) - \hat{\mathbf{e}}_\theta \cos(\theta+\theta_1)][\sin\theta_0 \cos\theta_1 \\ &\cdot \cos(\varphi-\varphi_0) - \cos\theta_0 \sin\theta_1] R_{s\parallel}(\theta_1) + \hat{\mathbf{e}}_\varphi[-\sin\theta_0 \\ &\cdot \sin(\varphi-\varphi_0)] R_{s\perp}(\theta_1)\}\mathrm{i}\omega\mu I l e^{\mathrm{i}kL_1}/(2\pi L_1). \end{aligned} \quad (5)$$

Similarly, by referring to (4), the field component $\mathbf{E}_2$ of the second propagation path can be obtained, which is reflected twice.

$$\begin{aligned}\mathbf{E}_2 = \{&(\hat{\mathbf{e}}_x \cos\theta_2 \cos\varphi + \hat{\mathbf{e}}_y \cos\theta_2 \sin\varphi - \hat{\mathbf{e}}_z \sin\theta_2) \\ &\cdot[\sin\theta_0 \cos\theta_2 \cdot \cos(\varphi-\varphi_0) - \cos\theta_0 \sin\theta_2] R_{s\parallel}(\theta_2) \\ &\cdot R_{g\parallel}(\theta_2) + \hat{\mathbf{e}}_\varphi[-\sin\theta_0 \sin(\varphi-\varphi_0)] R_{s\perp}(\theta_2) R_{g\perp}(\theta_2)\} \\ &\cdot \mathrm{i}\omega\mu I l e^{\mathrm{i}kL_2}/(4\pi L_2) \end{aligned} \quad (6)$$

where $R_{s\parallel}(\theta_2)$ and $R_{s\perp}(\theta_2)$ are the reflection coefficients of the different polarized electromagnetic waves at point $P'$ on the air-ionosphere interface; $\theta_2$ is the angle of incidence; $R_{g\parallel}(\theta_2)$ and $R_{g\perp}(\theta_2)$ are the reflection coefficients at point $Q$ on the air-ground interface. Converting all field components in directions $\hat{e}_x$, $\hat{e}_y$, and $\hat{e}_z$ in (6) to directions $\hat{e}_\theta$ and $\hat{e}_r$ again, we can further obtain

$$\begin{aligned}\mathbf{E}_2 = \{&[\hat{\mathbf{e}}_r \sin(\theta-\theta_2) + \hat{\mathbf{e}}_\theta \cos(\theta-\theta_2)] \cdot [\sin\theta_0 \cos\theta_2 \\ &\cdot \cos(\varphi-\varphi_0) - \cos\theta_0 \sin\theta_2] R_{s\parallel}(\theta_2) R_{g\parallel}(\theta_2) + \hat{\mathbf{e}}_\varphi[-\sin\theta_0 \\ &\cdot \sin(\varphi-\varphi_0)] R_{s\perp}(\theta_2) R_{g\perp}(\theta_2)\}\, \mathrm{i}\,\omega\mu I l e^{\mathrm{i}\,kL_2}/(4\pi L_2) \end{aligned} \quad (7)$$

The total propagation field $\mathbf{E}(R)$ contributed from two propagation paths is obtained as follows:

$$\mathbf{E}(R) = \mathbf{E}_1 + \mathbf{E}_2. \quad (8)$$

It should be noted that the two field components essentially represent the superposition of contributions from the electric dipole and its image source derived using the method of images. Taking the vertical dipole ($\theta_0 = 0$, $\varphi_0 = 0$) as a special case and setting both the observation point on the ground ($h_0 = 0$), (8) is consistent with that addressed in [9].

The field expression of the frequency-domain steady state by (8) is not applicable to Loran-C signals [10]. In the time domain, the electric-field component perpendicular to the ground is replaced by (9):

$$\begin{aligned}E_\theta(R) = &\mu I l/(2\pi L_1)[-\cos(\theta+\theta_1)][\sin\theta_0 \cos\theta_1 \\ &\cdot \cos(\varphi-\varphi_0) - \cos\theta_0 \sin\theta_1] \left|R_{s\parallel}(\theta_1)\right| \\ &\cdot[E_i(t - (k_0 L_1 - \varphi_{R_{s\parallel}(\theta_1)})/\omega)] \\ &+\mu I l/(2\pi L_2) \cos(\theta-\theta_2)[\sin\theta_0 \cos(\varphi-\varphi_0) \\ &\cdot \cos\theta_2 - \cos\theta_0 \sin\theta_2]|R_{s\parallel}(\theta_2)||R_{g\parallel}(\theta_2)| \\ &\cdot[E_i(t - (k_0 L_2 - \varphi_{R_{s\parallel}(\theta_2)} - \varphi_{R_{g\parallel}(\theta_2)})/\omega)]. \end{aligned} \quad (9)$$

where $\varphi_{R_{s\parallel}(\theta_1)}$, $\varphi_{R_{g\parallel}(\theta_1)}$, $\varphi_{R_{s\parallel}(\theta_2)}$, and $\varphi_{R_{s\parallel}(\theta_2)}$ are the phases of $R_{s\parallel}(\theta_1)$, $R_{g\parallel}(\theta_1)$, $R_{s\parallel}(\theta_2)$, and $R_{s\parallel}(\theta_2)$, and $Ei(t)$ is the normalized form of the Loran-C current derivative [19]. In a two-dimensional cylindrical coordinate system, LF sky waves excited by a vertically polarized dipole can be approximated as a transverse magnetic (TM) mode when propagating within the Earth-ionosphere waveguide. According to the field component relationships of TM waves in air, we can also obtain the magnetic field $H_\varphi$ [19]. However, the field components and propagation modes of a horizontally polarized dipole differ significantly from those of its vertically polarized counterpart.

For the one-hop sky-wave propagation over irregular terrain, (8) remains valid for calculating the electric field strength at various receiving heights. In Figure 1, for the $R$ above the irregular surface, the procedure for solving $\theta_1$ and $L_1$ remains fundamentally consistent, with only the parameter $h_0$ in (1) being replaced by $h_0 + h_m(d)$. Here, $h_m(d)$ denotes the vertical deviation of the irregular terrain from the reference horizontal ground. Parameters $L_2$ and $\theta_2$ are derived using the improved wave-hop theory [19]. By substituting these parameters into (8), the one-hop sky-wave field for an arbitrarily oriented dipole over irregular terrain is obtained.

## 3. SIMULATION ANALYSIS

In this section, numerical simulations are performed using the field strength of arbitrarily oriented electric dipoles located in the Earth-ionosphere waveguide. All three layers of the media were isotropic. In Figure 2, the Finite-Difference Time-Domain (FDTD) method was used to simulate and validate the one-hop sky-wave field strength excited by a vertical dipole ($\theta_0 = 0$, $\varphi_0 = \pi/2$) in the layered model. Two typical transmitters were selected, Loran-C signal sources and single-frequency sinusoidal signal sources [20], both operating at a frequency of 100 kHz and set to a uniform transmission power

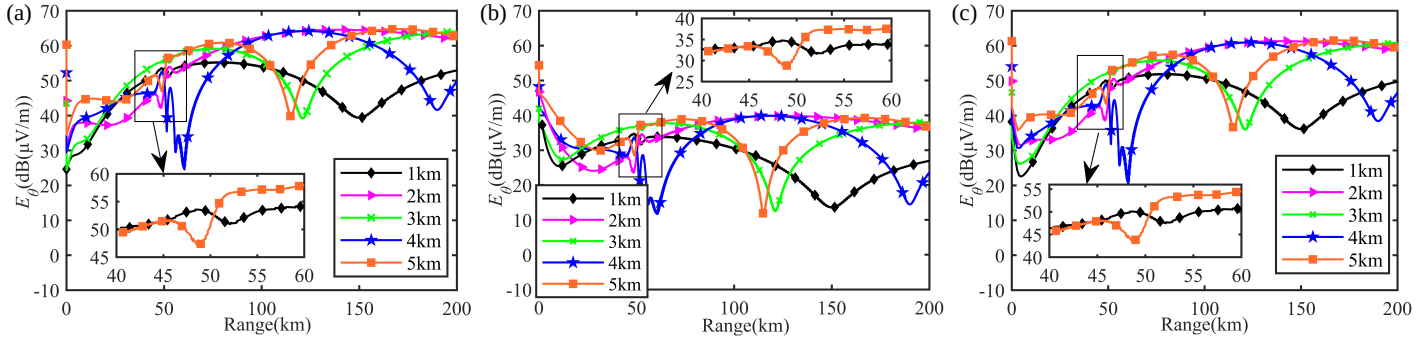


**FIGURE 3**. The one-hop sky-wave electric fields $E_\theta$ in the irregular Earth-ionosphere waveguide. (Sinusoidal signal). (a) Vertical dipole ($\theta_0 = 0$, $\varphi_0 = \pi/2$). (b) Horizontal dipole ($\theta_0 = \pi/2$, $\varphi_0 = 0$). (c) Oblique dipole ($\theta_0 = \pi/4$, $\varphi_0 = \pi/4$).

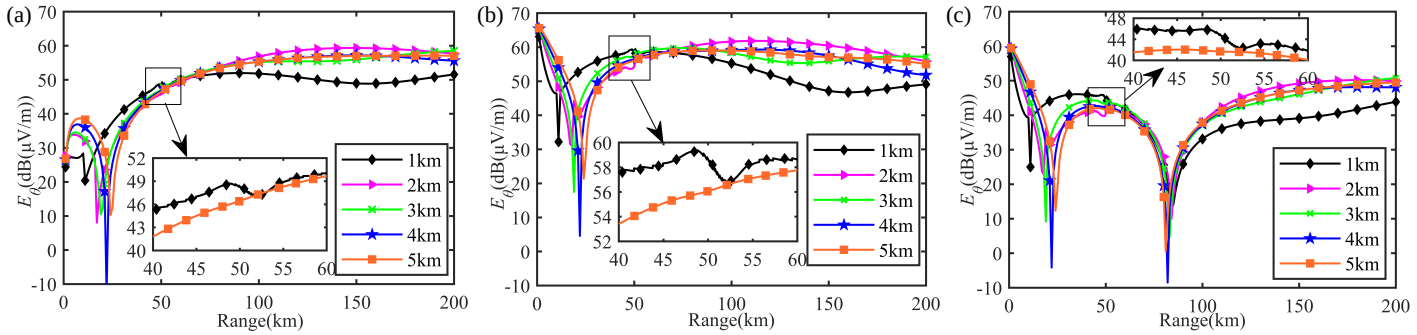


**FIGURE 4**. The one-hop sky-wave electric fields $E_\theta$ in the irregular Earth-ionosphere waveguide. (Loran-C signal). (a) Vertical dipole ($\theta_0 = 0$, $\varphi_0 = \pi/2$). (b) Horizontal dipole ($\theta_0 = \pi/2$, $\varphi_0 = 0$). (c) Oblique dipole ($\theta_0 = \pi/4$, $\varphi_0 = \pi/4$).

of 1 kW to ensure consistent excitation conditions throughout the simulation process. In the FDTD model, the grid size was $\Delta r = \Delta z = 18.75$ m, and the number of grids was approximately $12000 \times 4400$. The time step was set according to the Courant stability limit, $\Delta t = 3.125 \times 10^{-8}$ s. The total number of time steps was 40000. The $z$-axis of the model was the boundary of the symmetry axis, and the other boundaries were set to a perfectly matched layer boundary, $H = 60$ km. The maximum great-circle propagation distance $d$ was set to 200 km. A Gaussian mountain was positioned 50 km away from the transmitter. The horizontal extent of the mountain was approximately 10 km, and its peak height was 0.5 km. The conductivity of the ground was set to $\sigma_g = 3 \times 10^{-3}$ S/m, and its relative permittivity was $\varepsilon_{rg} = 13$. Air is taken as free space, with $\varepsilon_r = 1$ and $\sigma = 0$ S/m. The ionosphere was modeled as a perfect electric conductor. All transmitters were deployed on the Earth's surface.

In Figure 2, the lines with different markers represent the variation results of the one-hop sky-wave magnetic field $H_\varphi$ with the propagation distance obtained via the proposed method; the dashed lines denote the calculation results of the FDTD method. The variation of the received field strength from the ground to 5 km above the ground was investigated. The corresponding observation methods were adopted due to the differences in the inherent characteristics of the two transmitter types. For the sinusoidal signal, the peak value within the relatively stable time period before the arrival of the two-hop sky waves was selected as the field strength. In practical Loran-C system engineering, the negative peak value of the third carrier cycle of the Loran-C signal was used to measure field strength [10, 19]. The results demonstrate good agreement between the two methods. The results in Figure 2(b) of this study are consistent with those in Figure 6(a) of [19] and will not be repeated here.

Figures 3 and 4 show the strengths of the one-hop sky-wave electric field excited by sinusoidal signal sources and Loran-C signal sources with different polarization directions, respectively, obtained by the proposed method. In all cases, the receiving altitude range is from 1 km to 5 km. Specifically, Figures 3(a), 3(b), and 3(c) show the sky waves $E_\theta$ generated by the sinusoidal signal source in the vertical, horizontal, and oblique directions, respectively; correspondingly, Figures 4(a), 4(b), and 4(c) show the $E_\theta$ fields of the Loran-C signal sources under the three dipole orientations in the same order. For clarity, the zoom-in graphs in Figures 3 and 4 only show the electric field at receiving altitudes of 1 km and 5 km.

Figure 3 illustrates the variation in the frequency-domain electric field results with propagation distance, excited by dipoles of different polarization directions (at different receiving altitudes). Taking the receiving altitude of 1 km as an example, for propagation distances $d < 40$ km, the $E_\theta$ field of the one-hop sky wave excited by the vertical dipole exhibits an increasing amplitude. However, the one-hop sky waves $E_\theta$ excited in the horizontal and oblique dipoles first decrease and then increase. The electric field oscillates in mountainous areas, where $d$ is approximately between 40 km and 60 km. For

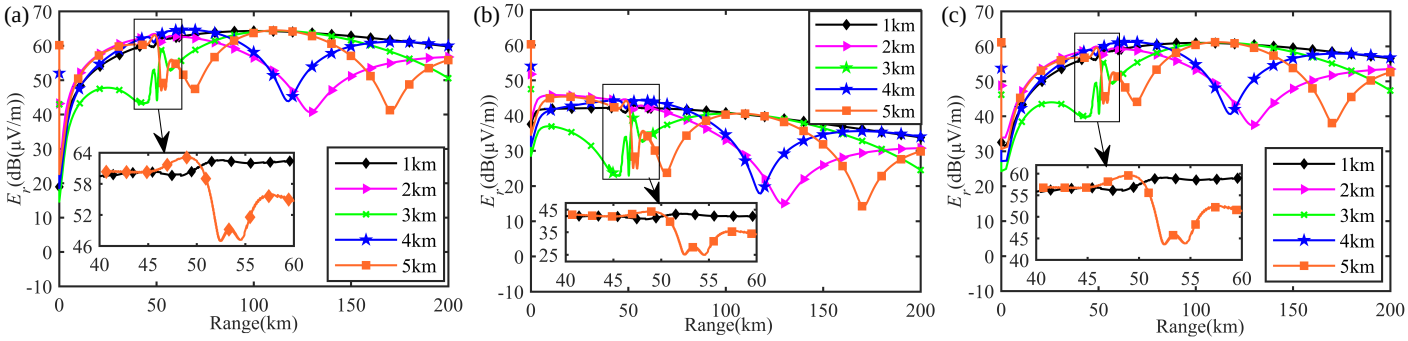


**FIGURE 5**. The one-hop sky-wave electric fields $E_r$ in the irregular Earth-ionosphere waveguide. (Sinusoidal signal). (a) Vertical dipole ($\theta_0 = 0$, $\varphi_0 = \pi/2$). (b) Horizontal dipole ($\theta_0 = \pi/2$, $\varphi_0 = 0$). (c) Oblique dipole ($\theta_0 = \pi/4$, $\varphi_0 = \pi/4$).

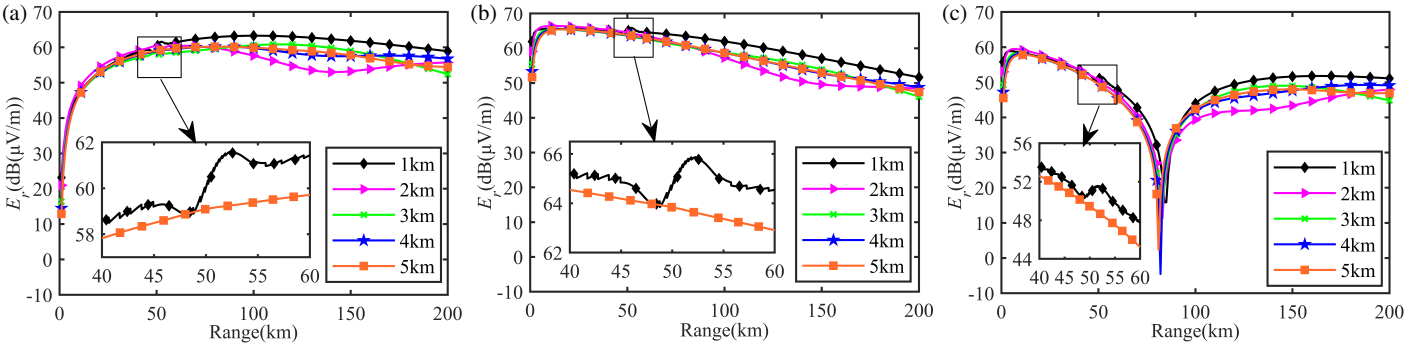


**FIGURE 6**. The one-hop sky-wave electric fields $E_r$ in the irregular Earth-ionosphere waveguide. (Loran-C signal). (a) Vertical dipole ($\theta_0 = 0$, $\varphi_0 = \pi/2$). (b) Horizontal dipole ($\theta_0 = \pi/2$, $\varphi_0 = 0$). (c) Oblique dipole ($\theta_0 = \pi/4$, $\varphi_0 = \pi/4$).

$d$ between 60 km and 200 km, the electric fields excited by the three dipoles show a trend of first decreasing and then increasing.

Figure 4 shows that the variation trend of the time-domain electric fields excited by dipoles of the same orientation at different reception heights is largely consistent as the propagation distance increases. As the propagation distance increases, the electric field $E_\theta$ of the one-hop sky wave excited by both vertical and horizontal dipoles initially decreases and then increases. All the fields decrease to a minimum at approximately 30 km, after which they increase and gradually exhibit relatively stable propagation characteristics. For the oblique dipole (Figure 4(c)), the electric field exhibits two minima as the propagation distance increases. The one-hop sky-wave electric field decays sharply at great-circle distances $d$ of approximately 80 km. Thereafter, for $d > 90$ km, the field strength gradually increases with distance and eventually stabilizes.

Figures 5 and 6 depict the one-hop sky-wave electric fields $E_r$ excited by sinusoidal signal sources and Loran-C signal sources with different polarization directions, respectively, obtained via the proposed method.

Near the mountainous region, the multipath effects at low receiving altitudes are the primary cause of oscillations in the one-hop sky-wave fields. The electric fields at different receiving heights show significant differences due to the combined effects of the emission source type, observation method, topographic relief, and receiving heights. Figures 3 and 5 show that the electric field curves at different altitudes within the mountainous region still exhibit distinct features corresponding to topographic variations. In contrast, in Figures 4 and 6, the field fluctuations gradually diminish as the reception height $h_0$ increases. This is mainly due to the ground-reflected wave arriving time lagging behind the observation time. The use of different observation methods resulted in significant discrepancies in the evaluated field strength at the same observation position.

## 4. CONCLUSION

In this study, a three-layer planar waveguide model consisting of the ionosphere, air, and ground was established. Based on the method of images and plane-wave reflection theory, the expression of the one-hop sky-wave radiation field of an arbitrarily oriented electric dipole in the Earth-ionosphere waveguide was derived and studied. The propagation formulation is subsequently extended to account for complex terrain effects, enabling its application to irregular surfaces. The radiation characteristics of two typical emission sources, Loran-C signal source and sinusoidal source, were studied, respectively. The propagation characteristics of one-hop sky waves from 100 kHz sources of various orientations were analyzed for different receiving heights within the Earth-ionosphere waveguide. The proposed method can also be extended to solve for multi-hop sky-wave fields in anisotropic ionospheric models [21]. It should be noted that the research on the application of exponential profile models or the International Reference Ionosphere (IRI) model to ionosphere modeling still needs to

be deepened. The proposed method is primarily applicable to irregular terrain with gentle slopes. The simplified treatment of ground reflection may introduce significant errors in terrains with large slopes [19]. Additionally, there are limitations in calculating the one-hop sky-wave field when the receiver is close to the ionosphere. Future work could consider the effects of the Earth's curvature, which were neglected in this study.

## ACKNOWLEDGEMENT

This study was supported by the National Natural Science Foundation of China (No. 62171265).

## APPENDIX A. TRANSFORMATION RELATION FOR UNIT VECTORS

The transformation relationship between the unit vector of the Cartesian coordinate system and that of the spherical coordinate system is as follows.

$$\begin{cases} \hat{\mathbf{e}}_x = \sin\theta\cos\varphi\hat{\mathbf{e}}_r + \cos\theta\cos\varphi\hat{\mathbf{e}}_\theta - \sin\varphi\hat{\mathbf{e}}_\varphi \\ \hat{\mathbf{e}}_y = \sin\theta\sin\varphi\hat{\mathbf{e}}_r + \cos\theta\sin\varphi\hat{\mathbf{e}}_\theta + \cos\varphi\hat{\mathbf{e}}_\varphi \\ \hat{\mathbf{e}}_z = \cos\theta\hat{\mathbf{e}}_r - \sin\theta\hat{\mathbf{e}}_\theta \end{cases} \tag{A1}$$

where $\theta$ is the polar angle of the observation point, and $\varphi$ is the azimuthal angle.

## REFERENCES

[1] Zhou, L., Y. Zheng, Z. Mu, X. Hu, X. Zhu, and L. He, "Distinction and characteristic analysis of different modes of low-frequency one-hop sky wave in the day-night transition area," *Acta Electronica Sinica*, Vol. 51, No. 7, 1964–1969, 2023.

[2] Kim, W., P.-W. Son, S. G. Park, S. H. Park, and J. Seo, "First demonstration of the Korean eLoran accuracy in a narrow waterway using improved ASF maps," *IEEE Transactions on Aerospace and Electronic Systems*, Vol. 58, No. 2, 1492–1496, 2022.

[3] Fan, X., Y. Zhang, P. R. Krehbiel, Y. Zhang, D. Zheng, W. Yao, L. Xu, H. Liu, and W. Lyu, "Application of ensemble empirical mode decomposition in low-frequency lightning electric field signal analysis and lightning location," *IEEE Transactions on Geoscience and Remote Sensing*, Vol. 59, No. 1, 86–100, 2021.

[4] Lü, X., X. Chen, W. Zhang, L. Gu, and W. Bao, "Acoustically actuated compact magnetoelectric antenna for low-frequency underwater communication," *IEEE Transactions on Antennas and Propagation*, Vol. 71, No. 11, 8493–8503, 2023.

[5] Niknam, K. and J. J. Simpson, "A review of grid-based, time-domain modeling of electromagnetic wave propagation involving the ionosphere," *IEEE Journal on Multiscale and Multiphysics Computational Techniques*, Vol. 6, 214–228, 2021.

[6] Bérenger, J.-P., "FDTD propagation of VLF-LF waves in the presence of ions in the Earth-ionosphere waveguide," *Annals of Telecommunications*, Vol. 75, No. 7, 437–446, 2020.

[7] Panyukov, A. V., "Estimation of the location of an arbitrarily oriented dipole under single-point direction finding," *Journal of Geophysical Research: Atmospheres*, Vol. 101, No. D10, 14 977–14 982, 1996.

[8] Wakai, N., N. Kurihara, and A. Otsuka, "Numerical method for calculating LF sky-wave, ground-wave and their resultant wave field strengths," *Electronics Letters*, Vol. 40, No. 5, 288–290, 2004.

[9] Wait, J. R., "A diffraction theory for lf sky-wave propagation," *Journal of Geophysical Research*, Vol. 66, No. 6, 1713–1724, 1961.

[10] Nazari, M. E. and W. Huang, "An analytical solution of electromagnetic radiation of a vertical dipole over a layered half-space," *IEEE Transactions on Antennas and Propagation*, Vol. 68, No. 2, 1181–1185, 2020.

[11] Karami, H., K. Sheshyekani, and F. Rachidi, "Mixed-potential integral equation for full-wave modeling of grounding systems buried in a lossy multilayer stratified ground," *IEEE Transactions on Electromagnetic Compatibility*, Vol. 59, No. 5, 1505–1513, 2017.

[12] Mu, Z., Q. Wang, L. Zhou, X. Hu, and L. He, "Comparison of low frequency multi-hop sky wave delay estimation algorithms," *Chinese Journal of Radio Science*, Vol. 37, No. 2, 244–250, 2022.

[13] Wait, J. R., "The ancient and modern history of EM ground-wave propagation," *IEEE Antennas and Propagation Magazine*, Vol. 40, No. 5, 7–24, 1998.

[14] Li, K., *Electromagnetic Fields in Stratified Media*, Zhejiang University Press, Hangzhou, China, 2009.

[15] Li, Z. X., H. R. Zeng, and K. Li, "Near field generated by a VLF magnetic dipole with arbitrary orientation in an anisotropic magnetoplasma," *IEEE Transactions on Plasma Science*, Vol. 51, No. 6, 1527–1539, 2023.

[16] Xu, H., T. Gu, J. Zheng, and K. Li, "LF sky wave propagation excited by a horizontal electric dipole towards understanding of its radiation mechanism," *Applied Computational Electromagnetics Society Journal (ACES)*, Vol. 33, No. 6, 657–664, 2018.

[17] Cao, L., B. Wei, and D.-B. Ge, "Computation of far radiation field of an arbitrarily oriented dipole above layered anisotropic half space," *Waves in Random and Complex Media*, Vol. 23, No. 4, 446–460, 2013.

[18] Zhou, L.-L., X.-Y. Hu, Z.-L. Mu, R. Zhang, and Y. Zheng, "Far-field calculation of an arbitrarily oriented electric dipole in horizontal layered confined space," *Acta Physica Sinica*, Vol. 71, No. 20, 1–7, 2022.

[19] Zhou, L., Y. Jiang, Z. Mu, Q. Wang, X. Hu, and L. He, "Study of Loran-C one-hop sky-wave fields at different altitudes above the ground," *IEEE Antennas and Wireless Propagation Letters*, Vol. 20, No. 12, 2368–2371, 2021.

[20] Xi, X., L. Zhou, J. Zhang, J. Liu, and L. Wang, "Combined IE-FDTD algorithm for long-range Loran-C ground-wave propagation," *IEEE Transactions on Antennas and Propagation*, Vol. 60, No. 8, 3802–3808, 2012.

[21] Zhou, L., Y. Zhang, Z. Mu, and X. Hu, "The calculation of the far-field radiation field of an electric dipole in anisotropic layered confined space," *Journal of Shaanxi University of Science & Technology*, Vol. 23, No. 4, 209–214, 2025.